

Article

# Interaction of Nanocomposites Based on the $\text{Fe}_m\text{O}_n\text{-SiO}_2$ System with an Electromagnetic Field in an Ultra-Wide Frequency Range

Kamil G. Gareev 

Department of Micro and Nanoelectronics, Saint Petersburg Electrotechnical University "LETI",  
197376 Saint Petersburg, Russia; kggareev@etu.ru

Received: 9 March 2020; Accepted: 28 May 2020; Published: 30 May 2020



**Abstract:** The article describes the interaction of nanocomposites based on the  $\text{Fe}_m\text{O}_n\text{-SiO}_2$  system with an electromagnetic field (radiation) in an ultra-wide frequency range 0– $10^{21}$  Hz. The development of the technique based on the sol–gel method for producing nanocomposites is described, which made it possible to achieve superparamagnetic properties in combination with low toxicity when used in vivo and in vitro and a high microwave absorption coefficient, which makes it possible to use the obtained nanocomposites in solving a wide range of practical problems. The most effective methods of exposure and threshold levels of the electromagnetic field, the corresponding modifications of the magnetic structure, crystalline structure and microstructure of nanocomposites are determined.

**Keywords:** sol–gel method; nanocomposites; iron oxide; silica; electromagnetic field; electromagnetic radiation; ultra-wide frequency range; interaction effects

## 1. Introduction

Soft chemistry synthesis method based on the sol–gel transition, well-known as the sol–gel method, have been used in nanotechnology for more than 50 years. Nevertheless, this method continues to be in demand and provides the opportunity to develop new classes of materials, including magnetic nanocomposites [1]. One of the most commonly indicated areas of application of magnetic nanocomposites obtained using the sol–gel method is biomedical fields such as in magnetic resonance imaging, magneto-controlled targeting, biosensing (e.g., immunoassays), RNA and DNA purification, gene cloning, cell separation and purification [2,3]. Although the basic principles of magnetism of nanoparticles (NPs) have been long since established, a general predictive picture of the magnetic properties of a given NPs or a family of NPs, is still lacking [4]. In addition to the features of magnetic properties, uncapped iron oxide NPs are highly reactive and prone to easy oxidation under ambient conditions damaging in magnet behavior and dispersion [5]. To avoid aggregation of magnetic nanoparticles, protection strategies have been developed to chemically stabilize the uncapped iron oxide NPs by grafting of or coating with organic species, including surfactants or polymers or coating with an inorganic layer, such as silica or carbon [6]. Stabilized iron oxide NPs are also used for magnetically mediated hyperthermia treatment that has been shown to be more effective than other forms of hyperthermia delivery [7].

For several years, nanocomposites based on the  $\text{Fe}_m\text{O}_n\text{-SiO}_2$  system ( $\text{Fe}_m\text{O}_n$  may be magnetite, maghemite or hematite depending on the synthesis conditions) were studied by the author, during which a method for producing a biocompatible water-based magnetic fluid with magnetite–silica NPs was proposed and the patent RU2639709 was obtained. As part of the work, samples of nanocomposites obtained under various synthesis conditions were studied, data on physicochemical and biologic characteristics were analyzed. In diagnostics of the crystalline structure, magnetic structure and

microstructure of samples, the most important place is occupied by methods based on physical effects arising from the interaction of electromagnetic fields (EMF) with nanocomposites in the frequency range from 0 to  $10^{21}$  Hz. This article is devoted to the main features of this interaction identified in the course of ongoing experimental studies.

The applicability of  $\text{Fe}_m\text{O}_n\text{-SiO}_2$  nanocomposites in various areas includes theranostics, producing electromagnetic shields and absorbers of electromagnetic waves, visualization of the local distribution of magnetic fields and detection of weak magnetic fields by changing the electrical impedance of the system.

The possibility of using  $\text{Fe}_m\text{O}_n\text{-SiO}_2$  nanocomposites in theranostics is due to the low cytotoxicity shown *in vitro* with respect to the culture of human umbilical vein endothelial cells [8] and hemocompatibility *in vivo* [9] due to the presence of a biologically inert silica shell, which significantly reduces cytotoxicity and improves the magnetic properties of nanocomposites due to the protection of magnetite from oxidation. In addition, the NPs themselves can be further modified with biocompatible fluorescent [10] or radioactive [11] tags, a cardioprotective drug [12] and an additional protein shell [13]. Visualization of processes in the body occurring in deep-lying tissues can be carried out using  $\text{Fe}_m\text{O}_n\text{-SiO}_2$  NPs due to the high nuclear magnetic resonance contrasting ability [14,15].

$\text{Fe}_m\text{O}_n\text{-SiO}_2$ -based nanocomposites can be used in conformal electromagnetic shields and electromagnetic wave absorbers due to high magnetic losses in the region of natural ferrimagnetic resonance and additional dielectric losses in a liquid or gel dispersion medium [16]. In this case, the value of microwave (MW) shielding coefficient in the frequency range 2–10 GHz is on average 5–10 dB with a thickness of the  $\text{Fe}_m\text{O}_n\text{-SiO}_2$  magnetic fluid layer of five millimeters [16].

$\text{Fe}_m\text{O}_n\text{-SiO}_2$  nanocomposites upon application of local gradient magnetic fields due to the appearance of dipole–dipole magnetostatic interactions of individual NPs and their aggregates [17] are able to form extended structures oriented along field lines [14,18], which allows visualizing the field distribution in the microscale. The effect of weak quasistatic magnetic field (QSMF), the strength of which is of the order of 100 A/m, can be detected using colloidal solutions of  $\text{Fe}_m\text{O}_n\text{-SiO}_2$  NPs by changing the electrical impedance of the system. In this case, the aggregation of NPs is reversible, and the state of the system is restored after the end of exposure, which can be used to create sensitive magnetic field sensors [19,20].

## 2. Materials and Methods

Aggregative stable colloidal solution of  $\text{Fe}_m\text{O}_n\text{-SiO}_2$  NPs in an aqueous medium was obtained in accordance with patent RU2639709. The method involves the precipitation of magnetite from an aqueous solution of ferric chloride (NevaReaktiv, Ltd., Saint Petersburg, Russia) and ferrous sulfate (NevaReaktiv, Ltd., Saint Petersburg, Russia) in an alkaline medium of ammonium hydroxide (NevaReaktiv, Ltd., Saint Petersburg, Russia), followed by the addition of 2 vol% tetraethyl orthosilicate (LenReaktiv, JSC, Saint Petersburg, Russia) and ultrasonic mixing using an ultrasonic dispenser Vibra-Cell VCX-130 (Sonics & Materials, Newtown, Connecticut, USA), after which the obtained NPs are washed and magnetically separated using N35 Nd–Fe–B magnet (Magnets and Systems, Ltd., Saint Petersburg, Russia). Immediately after synthesis of the NPs, their crystalline structure corresponds to magnetite according to the XRD data [17].

To study the shape and size of  $\text{Fe}_m\text{O}_n\text{-SiO}_2$  NPs, a layer was deposited on a glass substrate from the magnetic fluid, the surface image of which was obtained using a JSM-5800 scanning electron microscope (SEM) (JEOL Corp., Tokyo, Japan). Size distribution of  $\text{Fe}_m\text{O}_n\text{-SiO}_2$  NPs was analyzed by DLS using a Photocor Mini instrument (Photocor, Ltd., Moscow, Russia) with 200-fold dilution of magnetic fluid. The magnetic properties of  $\text{Fe}_m\text{O}_n\text{-SiO}_2$  NPs were studied by vibrating sample magnetometry of a dried residue obtained from magnetic fluid by using a 7410 Series instrument (Lake Shore Cryotronics, Inc., Westerville, Ohio, USA).

Interaction of nanocomposites based on the  $\text{Fe}_m\text{O}_n\text{-SiO}_2$  system with EMF was investigated on the basis of previous studies [8–33] of samples obtained by the author.

### 3. Results

#### 3.1. Physicochemical Properties of the Nanocomposites

The view of the obtained magnetic fluid containing nanocomposite  $\text{Fe}_m\text{O}_n\text{-SiO}_2$  NPs is shown in Figure 1a. The image of the surface of the layer deposited from magnetic fluid (diluted 200 times), obtained using a scanning electron microscope (SEM), is shown in Figure 1b. The deposited layer contains NPs and their aggregates with sizes in the range of 10–200 nm. The NPs sizes in the magnetic fluid correspond to a stable colloidal solution with a high value of the zeta-potential (at least 30 mV [20]). The large NPs observed may be aggregates formed during the drying of a droplet of magnetic fluid on the substrate. The size distribution of NPs obtained by dynamic light scattering (DLS) is shown in Figure 1c. As can be seen, the average NPs radius is about 70 nm, which corresponds to the SEM results. The saturation mass magnetization of the NPs is  $55 \text{ A}\cdot\text{m}^2/\text{kg}$  (Figure 1d), and the coercive force is  $400 \text{ A}/\text{m}$ .

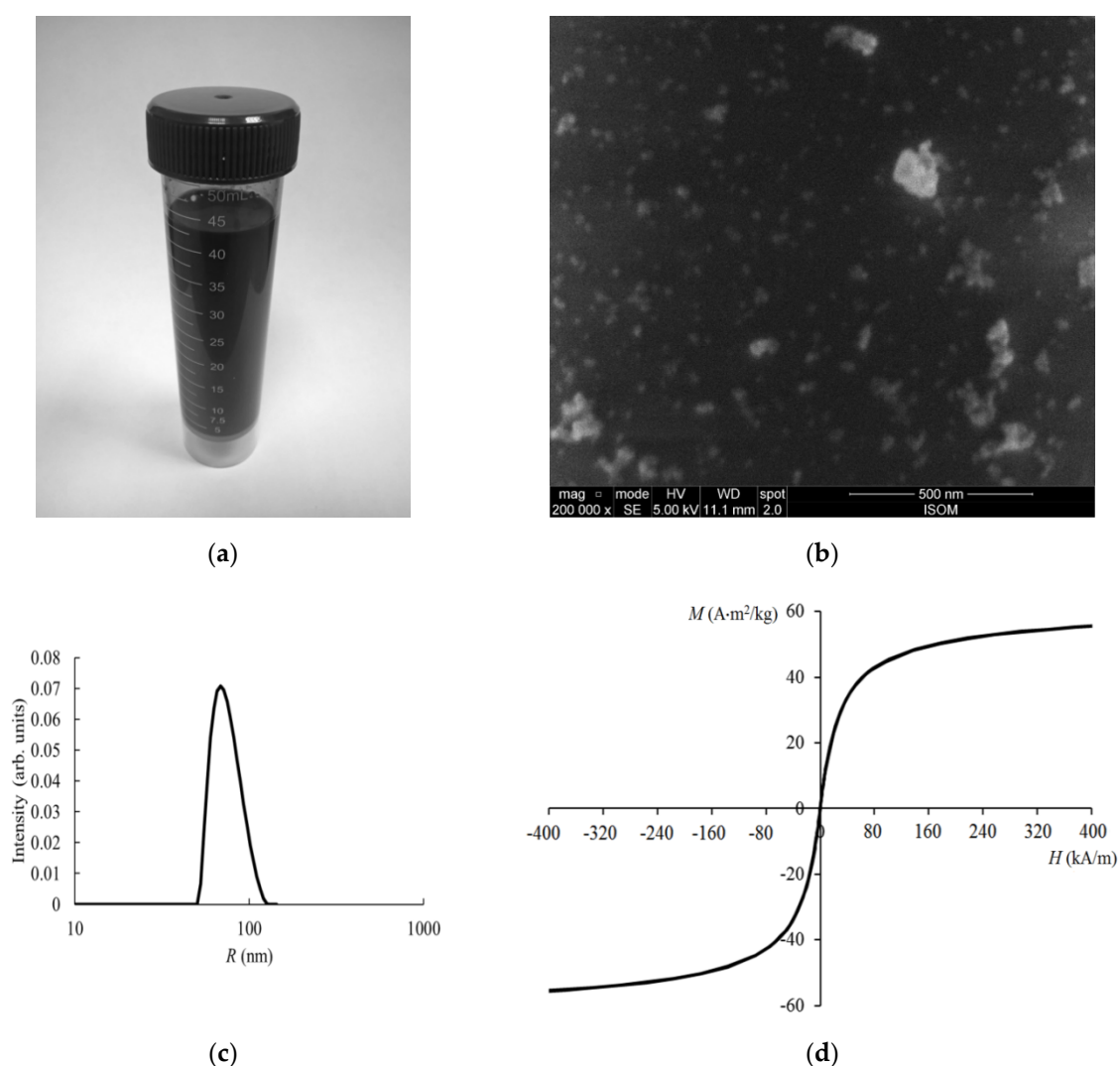


**Figure 1.** Physicochemical properties of the nanocomposites: (a) View of the obtained colloidal solution; (b) scanning electron microscope image; (c) nanoparticles radius distribution; (d) static magnetization reversal curve.

### 3.2. Physical Effects Observed in the Interaction of $\text{Fe}_m\text{O}_n\text{-SiO}_2$ Nanocomposites with EMF in an Ultra-Wide Frequency Range

During the research of  $\text{Fe}_m\text{O}_n\text{-SiO}_2$  nanocomposites, experimental methods were used based on the influence of an EMF of various types and frequencies: QSMF, alternating magnetic field (AMF), MW, terahertz (THz), far (FIR), middle (MIR) and near (NIR) infrared, visible (Vis), ultraviolet (UV), X-ray and  $\gamma$ -radiation covering a frequency range from 0 to  $10^{21}$  Hz. During the experiments, the samples were in solid (dry) and liquid (in a colloidal solution) aggregate states. One group of the observed effects is associated with a change in the magnetic structure, crystalline structure and microstructure of the samples, the other group of effects is not associated with a change in the structure and is used to diagnose the physicochemical properties of nanocomposites.

#### 3.2.1. Effects of Exposure to QSMF

QSMF with a frequency of 0–10 Hz, depending on the magnetic field strength, can affect the microstructure and magnetic structure of nanocomposites in the liquid and solid state (Table 1).

In the solid state in nanocomposites, static magnetization reversal, the formation of anhysteretic remanent magnetization (ARM), and the Zeeman effect (for observing electron paramagnetic resonance) are observed. Magnetization reversal of iron oxide NPs occurs during the measurement of static magnetization reversal curves using vibrating sample magnetometry when the external QSMF exceeds the strength value equal to the coercive force 160–500 A/m, depending on the method of producing the nanocomposite [8,20–24]. ARM was created using a SQUID magnetometer [24,25] in a constant field with strength of 80 A/m. The Zeeman effect was used to observe electron paramagnetic resonance (EPR) using a spectrometer in the QSMF strength range from 80 to 400 kA/m [26].

The effect of QSMF on nanocomposites in a liquid state leads to reversible and irreversible formation of aggregates from NPs, magnetization reversal of NPs and the Zeeman effect. The reversible formation of aggregates occurs upon short (up to 5 min) exposure to a constant magnetic field of strength 150–500 A/m during conductometric measurements [19,20]. The simultaneous application of QSMF with strength of 40–360 A/m and a longitudinal radio-frequency field when measuring the nonlinear component of the magnetization causes magnetization reversal of NPs [17]. An increase in the field strength to 10 kA/m and more leads to the formation of stable linear aggregates of NPs up to several tens of microns in length [15,18]. The high-strength QSMF due to the occurrence of Zeeman splitting allows one to observe nuclear magnetic resonance (NMR) on hydrogen nuclei (14 MHz in a field of 267 kA/m) in a colloidal solution of NPs when radiofrequency pulses are applied at the precession frequency of nuclear spins, the concentration of which affects the times relaxation of nuclear spins [14,15].

#### 3.2.2. Effects of Exposure to AMF

In the frequency range  $10^3\text{--}10^7$  Hz, when AMF is applied to the samples of nanocomposites in the solid state, the destruction of the ARM and dispersion of the initial magnetic permeability were observed in the experiments—and in the case of samples in the form of colloidal solutions of NPs—NMR (with simultaneous exposure to a transverse constant magnetic field with a strength of 267 kA/m) and nonlinearity of magnetization in the longitudinal QSMF.

The destruction of the ARM was carried out in a decreasing AMF with an amplitude of up to 40 kA/m [23,25]. Using the obtained ARM destruction curves, coercive spectra (distributions by the value of the coercive force) were constructed, which made it possible to refine the model of the internal structure of  $\text{Fe}_m\text{O}_n\text{-SiO}_2$  NPs and explain their magnetic properties [23].

**Table 1.** Physical effects observed during the interaction of nanocomposites based on the Fe<sub>m</sub>O<sub>n</sub>-SiO<sub>2</sub> system with various types of electromagnetic fields (EMF).

Frequency	EMF Type	Aggregate State	Type of Iron Oxide	Exposure Level	Observed Effects	Refs.
0–10 Hz	QSMF	solid	Fe <sub>3</sub> O <sub>4</sub> , γ-Fe <sub>2</sub> O <sub>3</sub>	160–500 A/m	magnetization reversal	[8,20–24]
				80–400 kA/m	Zeeman effect (for observing electron paramagnetic resonance (EPR))	[26]
				80 A/m	creation of anhysteretic remanent magnetization (ARM)	[24,25]
		liquid	Fe <sub>3</sub> O <sub>4</sub> , γ-Fe <sub>2</sub> O <sub>3</sub>	150–500 A/m	reversible aggregation of nanoparticles (NPs)	[19,20]
				16–160 kA/m	irreversible formation of linear aggregates of NPs	[15,18]
				40–360 A/m	magnetization reversal	[17]
			267 kA/m	Zeeman effect (for observing nuclear magnetic resonance (NMR))	[14,15]	
1 kHz	AMF	solid	Fe <sub>3</sub> O <sub>4</sub> , γ-Fe <sub>2</sub> O <sub>3</sub>	40 kA/m	destruction of ARM	[23,25]
10 <sup>2</sup> –10 <sup>6</sup> Hz		liquid	α-Fe <sub>2</sub> O <sub>3</sub>	100 A/m	dispersion of initial magnetic permeability	[27,28]
14 MHz		liquid	Fe <sub>3</sub> O <sub>4</sub> , γ-Fe <sub>2</sub> O <sub>3</sub>	1 kA/m	NMR	[14,15]
15.7 MHz		liquid	Fe <sub>3</sub> O <sub>4</sub> , γ-Fe <sub>2</sub> O <sub>3</sub>	1.1–1.6 kA/m	nonlinearity of the magnetization in a longitudinal field	[17]
10 GHz		solid	Fe <sub>3</sub> O <sub>4</sub> , γ-Fe <sub>2</sub> O <sub>3</sub>		EPR	[26]
0.1–18 GHz	MW	liquid	Fe <sub>3</sub> O <sub>4</sub> , γ-Fe <sub>2</sub> O <sub>3</sub>	1 mW	permeability dispersion	[16]
0.2–1.8 THz	THz	solid	Fe <sub>3</sub> O <sub>4</sub> , γ-Fe <sub>2</sub> O <sub>3</sub>	0.3 μW	dispersion of refractive index and absorption coefficient	[30]
12–120 THz	FIR and MIR	solid	Fe <sub>3</sub> O <sub>4</sub> , γ-Fe <sub>2</sub> O <sub>3</sub>	0.12–0.14 eV, 1.2 mW	vibration absorption of Si–O–Si groups	[8,22,24]
10 <sup>14</sup> –10 <sup>15</sup> Hz	UV, Vis, NIR	solid	Fe <sub>3</sub> O <sub>4</sub> , α-Fe <sub>2</sub> O <sub>3</sub> , γ-Fe <sub>2</sub> O <sub>3</sub>	0.3–0.9 mw (5–15 kW/cm <sup>2</sup> )	Raman scattering	[31,32]
				1–2 mW (17–35 kW/cm <sup>2</sup> )	phase transition magnetite → maghemite → hematite	[29,31,32]
		liquid	Fe <sub>3</sub> O <sub>4</sub> , γ-Fe <sub>2</sub> O <sub>3</sub>	2–6 eV	intrinsic absorption in iron oxide and in silica	[14,15]
				4–20 mW	Dynamic light scattering	[8,20,23,33]
10 <sup>18</sup> –10 <sup>21</sup> Hz	X-ray	solid	Fe <sub>3</sub> O <sub>4</sub> , α-Fe <sub>2</sub> O <sub>3</sub> , γ-Fe <sub>2</sub> O <sub>3</sub>	5.4–8.0 keV (0.154–0.229 nm)	X-ray diffraction on the crystal lattice	[17,23,27,28,31]
	γ		Fe <sub>3</sub> O <sub>4</sub> , γ-Fe <sub>2</sub> O <sub>3</sub>	14.4 keV, 20 mCi	Mössbauer effect	[23]
			Fe <sub>3</sub> O <sub>4</sub> , γ-Fe <sub>2</sub> O <sub>3</sub>	1.17–1.33 MeV, 10 <sup>6</sup> rad	radiation-induced phase transition magnetite → maghemite	[32]

The frequency spectra of the effective initial magnetic permeability of nanocomposites based on the  $\text{Fe}_m\text{O}_n\text{-SiO}_2$  system with the addition of nickel and cobalt oxides were constructed using impedance measurements [27,28]. The nature of the frequency dispersion of the initial magnetic permeability of nanocomposites depends on the ratio between iron oxide and nickel and cobalt oxides. The decrease in magnetic permeability with increasing frequency is minimal with the predominance of iron oxide, which can be caused by the high electrical resistivity of hematite, which has a band gap of about 2.1 eV [29].

NMR was observed using a Spin Track NMR relaxometer (Resonance Systems LLC, Yoskar-Ola, Russia) at a frequency of 14 MHz in a constant magnetic field of 267 kA/m [14,15]. As described above, in the presence of high-strength QSMF,  $\text{Fe}_m\text{O}_n\text{-SiO}_2$  NPs form linear aggregates, as a result of which the relaxation times and relaxation efficiency were unstable in the dynamics of the experiment and after a few weeks a decrease in the indicated characteristics was observed. Moreover, at the initial time (before long-term exposure to a high-strength magnetic field), the relaxation efficiency was at the level of  $300\text{--}400 \text{ L}\cdot\text{mM}^{-1}\cdot\text{s}^{-1}$ , which corresponds to a high contrasting ability for magnetic resonance imaging [14].

The nonlinear component of the magnetization in the longitudinal QSMF was measured in colloidal solutions of NPs at their low concentration (at a level of 1 mM/L), which corresponds to the solution concentrations used for magnetic resonance imaging [14] and does not allow the study of magnetostatic characteristics by vibrating sample magnetometry even during freezing samples in liquid nitrogen [17]. Under the influence of AMF with a frequency of 15.7 MHz and an amplitude of 1.1–1.6 kA/m in the longitudinal QSMF with an amplitude of 24 kA/m, the field dependences of the second magnetization harmonic were obtained, as well as the temperature and frequency dependences of the coercive force of NPs. Their superparamagnetic behavior was established with a blocking temperature of 240 K at a QSMF frequency of 1.3 Hz and a blocking diameter of about 20 nm with an average magnetite crystallite size of about 8 nm.

### 3.2.3. Effects of Exposure to MW

The nanocomposites based on the  $\text{Fe}_m\text{O}_n\text{-SiO}_2$  system in the solid state in the form of layers deposited on a glass substrate and in the form of magnetic fluid were subjected to MW in the frequency range 0.1–18.0 GHz.

To study the effect of  $\gamma$ -radiation on the crystalline and magnetic structure of iron oxide, the  $\text{Fe}_m\text{O}_n\text{-SiO}_2$  nanocomposite in the form of a dry powder was subjected to MW at a frequency of 10 GHz using an EPR spectrometer. The presence of bands in the g-factor region equal to 2.04 and 2.8, which are due to the oxidation of iron from the  $\text{Fe}^{2+}$  state to  $\text{Fe}^{3+}$  and the dipole–dipole interaction between iron oxide crystallites inside the nanocomposite, respectively, was established [26].

$\text{Fe}_m\text{O}_n\text{-SiO}_2$  NPs' magnetic fluid for experiments on interaction with electromagnetic fields in the frequency range up to 18 GHz was placed in a special cuvette made of radiotransparent polymer placed on a coplanar waveguide and between horn antennas [16]. It was found that in the frequency range above 7 GHz, absorption of up to 95% of the MW energy was observed.

### 3.2.4. Effects of Exposure to THz

$\text{Fe}_m\text{O}_n\text{-SiO}_2$  NPs dispersed in compressed KBr pellets in an amount of 1–2 mas% were exposed to THz radiation in the frequency range 0.2–1.8 THz using a spectrometer created at ITMO University [30]. The spectra of the refractive index obtained showed no significant features, while the absorption coefficient spectrum had a characteristic maximum of  $16 \text{ cm}^{-1}$  at a frequency of 1.3 THz the absorption coefficient of a reference sample from pure KBr at this frequency was  $4 \text{ cm}^{-1}$ , and the absorption coefficient of the sample containing NPs of iron oxide–hydroxide without silica was  $12 \text{ cm}^{-1}$ . Thus, the characteristic maximum can be explained by the presence of magnetite, which was protected from oxidation by a silica shell [30].

### 3.2.5. Effects of Exposure to FIR and MIR

Influence of EMF in the frequency range 12–120 THz (wave numbers 400–4000  $\text{cm}^{-1}$ ) on the  $\text{Fe}_m\text{O}_n\text{-SiO}_2$  NPs were carried out using an IR Fourier transform spectrometer [8,22,24]. The samples were compressed KBr-based tablets containing 1–2 mas% NPs. During the experiments, it was found that the nanocomposite intensively absorbs IR radiation with a quantum energy of 0.12–0.14 eV, which corresponds to the vibrational mode of the Si–O–Si group, while the optical density in the region of this maximum was three times higher than in the band absorption of OH groups, which can be used for local heating using an IR laser [24].

### 3.2.6. Effects of Exposure to NIR, Vis and UV

This group of effects was observed using optical diagnostic methods in samples of nanocomposites in liquid (colloidal solutions of  $\text{Fe}_m\text{O}_n\text{-SiO}_2$  NPs) and solid (layers of  $\text{Fe}_m\text{O}_n\text{-SiO}_2$  xerogel on glass substrates and layers deposited from a colloidal solution) states.

The layers of nanocomposites that underwent heat treatment at 600 °C were studied for transmission in the wavelength range of 390–990 nm. From the obtained data, the optical band gap of 2.1 eV was determined, corresponding to hematite and maghemite, and the transmission in the intrinsic absorption band of iron oxide was inversely proportional to the number of deposited layers [29].

The layers of  $\text{Fe}_m\text{O}_n\text{-SiO}_2$  NPs deposited from a colloidal solution were studied using optical absorption spectroscopy using G. Mie's theory [31]. Six absorption bands were discovered, which can be caused by iron oxide crystallites of different size fractions from 1.5 to 3 nm immobilized on the surface of silica globules.

In addition, the obtained samples of nanocomposite layers were subjected to local exposure to focused laser radiation with a spot diameter of 1–2  $\mu\text{m}$  at a wavelength of 532 nm using a Raman spectrometer [31,32]. Two different effects were observed in nanocomposites depending on the power of the incident radiation: Raman scattering and phase transition magnetite  $\rightarrow$  maghemite  $\rightarrow$  hematite. At a laser power of 0.3–0.9 mW (power density on the sample 5–15  $\text{kW}/\text{cm}^2$ ), the presence of weakly crystallized phases of magnetite and maghemite, respectively, was confirmed by characteristic Raman shifts in the range of 670–700  $\text{cm}^{-1}$  and 1400  $\text{cm}^{-1}$ , respectively. With increasing radiation power, a phase transition of magnetite and maghemite to hematite was observed, and the position of the band attributed to vibrations with  $A_{1g}$  symmetry corresponded to iron oxide crystallite sizes less than 10 nm, which indirectly confirms the results obtained by other methods [32]. It was also found that the threshold radiation power at which the phase transition occurs depends on the content of tetraethyl orthosilicate in the sol, from which silica was obtained.

Colloidal solutions of NPs were studied by spectrophotometry in the wavelength range of 190–1000 nm [14,15]. The spectra show a decrease in the transmittance at wavelengths less than 600 nm, which corresponds to the band gap of maghemite. The sharp decrease in transmittance when the wavelength approaches 200 nm was explained by the presence of amorphous silica. Kinetic measurements were also carried out at a fixed wavelength of 400 nm, and the sedimentation time of NPs was estimated from these results. The average size obtained on the basis of sedimentation curves was 100–300 nm, which generally corresponds to SEM and atomic force microscopy data [14].

The impact of laser radiation at a wavelength of 633–638 nm on the colloidal solution of NPs was provided using particle size analyzers based on the DLS method [8,23,29,33]. In the course of the studies, it was found that NPs obtained both in one- and two-stage methods [8,22] were characterized by an average particle size of 100–200 nm, and when diluting a stable magnetic fluid based on  $\text{Fe}_m\text{O}_n\text{-SiO}_2$  NPs, necessary for measuring by the DLS method, there was a loss of aggregate and sedimentation stability after several days, that is, dilution acts as a factor similar to a high-strength QSMF [14]. Later, the possibility of the formation of two dimensional fractions in a colloidal solution was revealed: in addition to NPs or their aggregates with sizes of 100–200 nm, there were formations of sizes of the

order of 20–30 nm, which, according to theoretical modeling, were also formed from several crystallites of iron oxide [20,23].

### 3.2.7. Effects of Exposure to X-ray

X-ray radiation with photon energies of 5.4 and 8.0 keV (radiation wavelength for the  $\text{CrK}_\alpha$  line was 0.229 nm and wavelength for  $\text{CuK}_\alpha$  line was 0.154 nm) on nanocomposites based on the  $\text{Fe}_m\text{O}_n\text{-SiO}_2$  system was carried out during the X-ray phase analysis of samples in solid state [17,23,27,28,31]. As a result of X-ray diffraction on the crystal lattice of iron oxides, as well as Ni, Co, Mn, Zn, Y and Er oxides, the phase composition of nanocomposites, stoichiometry, crystallinity and average crystallite size were determined, including in those cases when the internal structure's analysis using other available methods was not possible [17,23]. The studies carried out made it possible to establish the influence of various factors, including the temperature and duration of heat treatment, the ratio between the oxide precursors in the sol on the crystalline structure of nanocomposites.

### 3.2.8. Effects of Exposure to $\gamma$ -Radiation

$\gamma$ -radiation with a quantum energy of 14.4 keV (source— $^{57}\text{Co}$ , activity of 20 mCi) and 1.17–1.33 MeV (source— $^{60}\text{Co}$ , dose of  $10^6$  rad) can cause Mössbauer effect (nuclear gamma resonance) in  $\text{Fe}_m\text{O}_n\text{-SiO}_2$  nanocomposites and radiation-induced phase transition of magnetite to maghemite, respectively.

When conducting Mössbauer spectroscopy, it is possible to establish the chemical environment of iron cations and, thereby, determine the crystalline phases of iron oxides and their magnetic state, which was used in the analysis of the  $\text{Fe}_m\text{O}_n\text{-SiO}_2$  NPs to confirm the superparamagnetic state of individual iron oxide crystallites with sizes of about 10 nm, which transit to a stable single domain state as a result of the dipole–dipole interaction inside the composite NPs [23].

The radiation-induced phase transition of magnetite to maghemite was carried out as part of the study of  $\text{Fe}_m\text{O}_n\text{-SiO}_2$  nanocomposites by optical methods (optical absorption spectroscopy and Raman spectroscopy) [31]. Important differences between the effects of  $\gamma$ -radiation on the crystalline structure of iron oxide and the effects of laser radiation are its non-local nature (the sample was exposed as a whole, in contrast to a region of several  $\mu\text{m}^2$  in the case of local laser irradiation) and the high cost of sources while maintaining the magnetic properties of the sample was a further transition from maghemite to hematite with antiferromagnetic properties, in the absence of a thermal effect (the transition temperature lies in the range 400–500 °C [32]) coming off.

## 4. Discussion

Thus, under the influence of EMF of various types and frequencies, a number of physical effects were observed in the obtained nanocomposites (Figure 2 Figure 3 Figure 4), which have both scientific and practical significance. Moreover, one group of the observed effects is not accompanied by a change in the crystalline structure, magnetic structure or microstructure of the samples, which made it possible to use them for the diagnosis of the physicochemical properties of nanocomposites. The emergence of another group of effects leads to a change in the structural characteristics of the samples and therefore these effects can be used to directionally change the physicochemical properties in the practical use of nanocomposites in various fields of science and technology.

The research has shown that when a certain level of EMF influence on nanocomposites is exceeded, a directional change in their magnetic structure, crystalline structure and microstructure is possible: the formation of stable linear aggregates of NPs, a change in the magnetic state and phase transitions of iron oxides.

The change in the microstructure of the nanocomposites represented the formation of linear aggregates under the influence of high-strength QSMF (Table 2). When the threshold level of exposure, corresponding to the strength of the QSMF  $\sim 10^4$  A/m (Figure 2), is exceeded, the formation of stable aggregates sedimenting in a colloidal solution was observed [14,18].

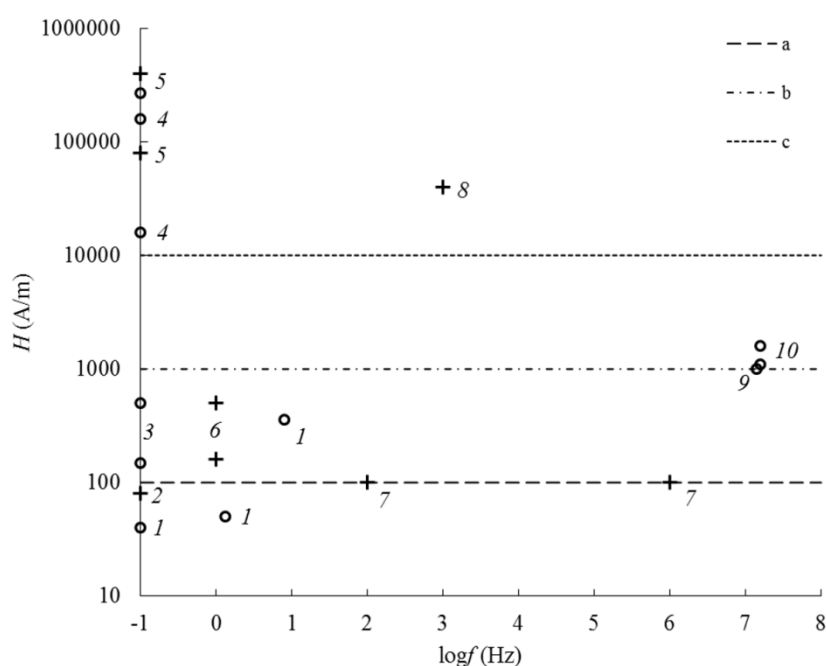


**Figure 2.** Frequency dependence of the magnetic field strength during the interaction of electromagnetic field with nanocomposites based on the  $\text{Fe}_m\text{O}_n\text{-SiO}_2$  system in the frequency range  $10^{-1}$ – $10^8$  Hz: 1—magnetization reversal (liquid), 2—formation of anhysteretic remanent magnetization (ARM) (solid), 3—reversible aggregation (liquid), 4—irreversible formation of linear aggregates (liquid), 5—Zeeman effect (solid, liquid), 6—magnetization reversal (solid), 7—dispersion of initial magnetic permeability (solid), 8—destroying ARM (solid), 9—nuclear magnetic resonance (liquid), 10—nonlinearity magnetization in a longitudinal field (liquid). “+” Corresponds to a solid state, “o”—to a liquid state. a is the threshold level of change in the magnetic structure of the sample in the liquid state, b is the threshold level of change in the magnetic structure of the sample in the solid state, c is the threshold level of change in the microstructure of the sample in the liquid state.

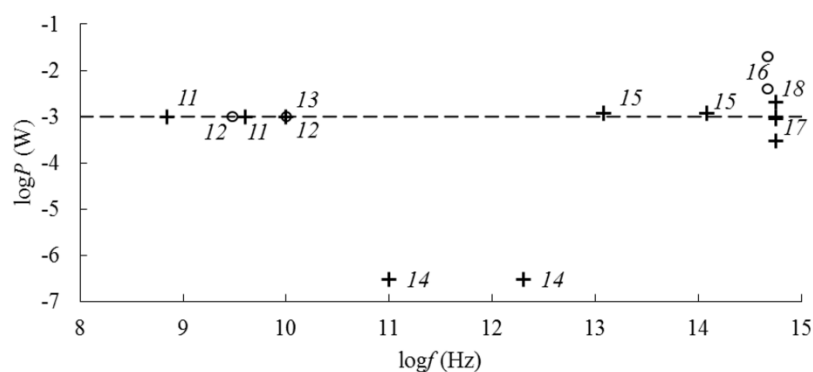


**Figure 3.** Frequency dependence of electromagnetic field power when interacting with nanocomposites based on the  $\text{Fe}_m\text{O}_n\text{-SiO}_2$  system in the frequency range  $10^8$ – $10^{15}$  Hz: 11—natural ferrimagnetic resonance (solid), 12—magnetic permeability dispersion (liquid), 13— electron paramagnetic resonance (solid), 14—dispersion of the refractive index and absorption coefficient (solid), 15—vibration absorption of Si–O–Si groups (solid), 16— dynamic light scattering (liquid), 17—Raman scattering (solid), 18—phase transition magnetite → maghemite → hematite (solid). “+” corresponds to a solid state, “o” corresponds to a liquid state. The dashed line corresponds to the threshold level of change in the crystalline structure.

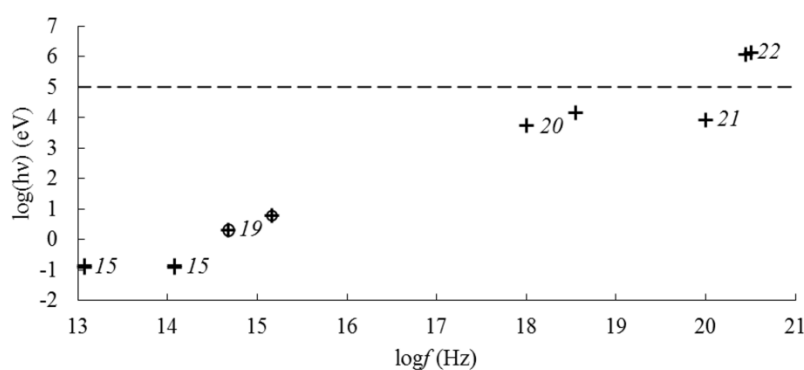


**Figure 4.** Frequency dependence of the characteristic energy of quanta during the interaction of electromagnetic field with nanocomposites based on the  $\text{Fe}_m\text{O}_n\text{-SiO}_2$  system in the frequency range  $10^{13}\text{--}10^{21}$  Hz: 15—absorption on vibrations of Si–O–Si groups (solid), 19—intrinsic absorption in iron oxide and silica (solid, liquid), 20—X-ray diffraction on the crystal lattice (solid), 21—Mössbauer effect (solid), 22—radiation-induced phase transition magnetite  $\rightarrow$  maghemite (solid). “+” corresponds to a solid state, “○” corresponds to a liquid state. The dashed line corresponds to the threshold level of change in the crystalline structure.

**Table 2.** Threshold levels of electromagnetic field exposure when modifying the structure of nanocomposites.

Modified Structure	State	Modification Method	Threshold Level	Refs.
Microstructure	Liquid	Influence of quasistatic magnetic field	$10^4$ A/m	[14,18]
Magnetic structure	Liquid		$10^2$ A/m	[17]
	Solid		$10^3$ A/m	[8,20–24]
Crystalline structure	Liquid	Local laser heating $\gamma$ -irradiation	$10^{-3}$ W	[19,31,32]
			$10^5$ eV	[26,32]

The change in the magnetic state of the nanocomposites was carried out by the influence of QSMF (Table 2). For samples in the liquid state, the threshold exposure level corresponded to a field strength of  $\sim 10^2$  A/m (Figure 2), while the direction of magnetization in  $\text{Fe}_m\text{O}_n\text{-SiO}_2$  NPs changed [17]. The magnetization reversal of nanocomposites in the solid state occurred when the threshold level of exposure corresponding to the strength of the QSMF  $\sim 10^3$  A/m was exceeded (Figure 2) [8,20–24].

The change in the crystalline structure of nanocomposites consisted in the phase transition of magnetite to hematite or maghemite upon local exposure to laser radiation or  $\gamma$ -radiation on nanocomposites in the form of layers or powders, respectively (Table 2). A laser power of  $\sim 10^{-3}$  W (power density on the sample  $\sim 10^4$  W/cm<sup>2</sup>) corresponded to the threshold level of exposure (Figure 3) to complete the formation of hematite [19,31,32]. The phase transition of magnetite to maghemite under the influence of  $\gamma$ -radiation occurred at a level of exposure corresponding to quantum energy of  $\sim 10^5$  eV and a dose of  $10^6$  rad (Figure 4) [26].

A directed modification of the structure of nanocomposites can be used, for example, to create theranostics' agents that, after being delivered to a targeted area and drug release, are converted to an antiferromagnetic state due to the transition of magnetite to hematite. Using the same principle, it is possible to create layers that absorb MW, which, if necessary, become radiotransparent due to the formation of hematite, which, unlike magnetite, is a dielectric for a transmitted EMF due to its high electrical resistivity and the absence of magnetic losses.

## 5. Conclusions

In the course of experimental studies, techniques based on the sol–gel method were developed for producing nanocomposites based on the  $\text{Fe}_m\text{O}_n\text{-SiO}_2$  system and a patent for the invention was obtained. The synthesis conditions corresponding to the superparamagnetic state of nanocomposites—the joint

deposition of iron oxide and silica from a solution of precursors at room temperature—are determined. Using state-of-the-art diagnostic techniques for the magnetic structure, crystalline structure and microstructure of samples based on exposure to EMF in the frequency range from 0 to  $10^{21}$  Hz, various physical effects were observed, which made it possible to obtain reliable information about the properties of nanocomposites and also to control their structure when the exposure level changes. QSMF was applied to modify the magnetic structure and microstructure of the samples. The crystalline structure was modified by local exposure to laser radiation and exposure to  $\gamma$ -radiation.

The research confirms the promise of nanocomposites based on the  $\text{Fe}_m\text{O}_n\text{-SiO}_2$  system in solving a wide range of technical and biomedical problems.

**Funding:** This research received no external funding.

**Conflicts of Interest:** The author declares no conflict of interest.

## References

1. Klein, L.; Jitianu, A.; Aparicio, M. (Eds.) *Handbook of Sol-Gel Science and Technology*, 2nd ed.; Springer International Publishing: Cham, Switzerland, 2018; pp. 9–15. ISBN 978-3-319-32101-1.
2. Owens, G.J.; Singh, R.K.; Foroutan, F.; Alqaysi, M.; Han, C.-M.; Mahapatra, C.; Kim, H.-W.; Knowles, J.C. Sol-gel based materials for biomedical applications. *Prog. Mater. Sci.* **2016**, *77*, 1–79. [[CrossRef](#)]
3. Katz, E. Synthesis, properties and applications of magnetic nanoparticles and nanowires—A brief introduction. *Magnetochemistry* **2019**, *5*, 61. [[CrossRef](#)]
4. Barrera, G.; Tiberto, P.; Allia, P.; Bonelli, B.; Esposito, S.; Marocco, A.; Pansini, M.; Leterrier, Y. Magnetic properties of nanocomposites. *Appl. Sci.* **2019**, *9*, 212. [[CrossRef](#)]
5. Gul, S.; Khan, S.B.; Rehman, I.U.; Khan, M.A.; Khan, M.I. A Comprehensive review of magnetic nanomaterials modern day theranostics. *Front. Mater.* **2019**, *6*, 179. [[CrossRef](#)]
6. Kalia, S.; Kango, S.; Kumar, A.; Haldorai, Y.; Kumari, B.; Kumar, R. Magnetic polymer nanocomposites for environmental and biomedical applications. *Colloid. Polym. Sci.* **2014**, *292*, 2025–2052. [[CrossRef](#)]
7. Hauser, A.K.; Wydra, R.J.; Stocke, N.A.; Anderson, K.W.; Hilt, J.Z. Magnetic nanoparticles and nanocomposites for remote controlled therapies. *J. Control. Release* **2015**, *219*, 79–94. [[CrossRef](#)]
8. Toropova, Y.G.; Golovkin, A.S.; Malashicheva, A.B.; Korolev, D.V.; Gorshkov, A.N.; Gareev, K.G.; Afonin, M.V.; Galagudza, M.M. In vitro toxicity of  $\text{Fe}_m\text{O}_n$ ,  $\text{Fe}_m\text{O}_n\text{-SiO}_2$  composite, and  $\text{SiO}_2\text{-Fe}_m\text{O}_n$  core-shell magnetic nanoparticles. *Int. J. Nanomed.* **2017**, *12*, 593–603. [[CrossRef](#)]
9. Toropova, Y.G.; Pechnikova, N.A.; Zelinskaya, I.A.; Korolev, D.V.; Gareev, K.G.; Markitantova, A.S.; Bogushevskaya, V.D.; Povolotskaya, A.V.; Manshina, A.A. Hemocompatibility of magnetic magnetite nanoparticles and magnetite-silica composites in vitro. *Bull. Sib. Med.* **2018**, *17*, 157–167. [[CrossRef](#)]
10. Gareev, K.G.; Babikova, K.Y.; Postnov, V.N.; Naumisheva, E.B.; Korolev, D.V. Fluorescence imaging of the nanoparticles modified with indocyanine green. *J. Phys. Conf. Ser.* **2017**, *917*, 042008. [[CrossRef](#)]
11. Korolev, D.V.; Postnov, V.N.; Evreinova, N.V.; Babikova, K.Y.; Naumysheva, E.B.; Shulmeister, G.A.; Magruk, M.A.; Mishanin, V.I.; Toropova, Y.G.; Gareev, K.G.; et al. Synthesis of magnetic nanoparticles with radiopaque marker. *Russ. J. Gen. Chem.* **2018**, *88*, 2698–2701. [[CrossRef](#)]
12. Korolev, D.V.; Evreinova, N.V.; Zakharova, E.V.; Gareev, K.G.; Naumysheva, E.B.; Postnov, D.V.; Postnov, V.N.; Galagudza, M.M. Phosphocreatine immobilization of the surface of silica and magnetite nanoparticles for targeted drug delivery. *Russ. Chem. Bull.* **2019**, *68*, 1096–1101. [[CrossRef](#)]
13. Korolev, D.V.; Gareev, K.G.; Zorin, V.N.; Evreinova, N.V.; Postnov, V.N.; Romanova, T.N. Synthesis of glycidoxy spacer on the surface of magnetic nanoparticles and immobilization of albumin. *J. Phys. Conf. Ser.* **2019**, *1410*, 012069. [[CrossRef](#)]
14. Bogachev, Y.V.; Chernenco, J.S.; Gareev, K.G.; Kononova, I.E.; Matyushkin, L.B.; Moshnikov, V.A.; Nalimova, S.S. The study of aggregation processes in colloidal solutions of magnetite–silica nanoparticles by NMR relaxometry, AFM, and UV–Vis-Spectroscopy. *Appl. Magn. Reson.* **2014**, *45*, 329–337. [[CrossRef](#)]
15. Bogachev, Y.V.; Gareev, K.G.; Matyushkin, L.B.; Moshnikov, V.A.; Naumova, A.N. Study of magnetite nanoparticle suspensions by photometry and NMR relaxometry. *Phys. Solid State* **2013**, *55*, 2313–2317. [[CrossRef](#)]

16. Gareev, K.G.; Luchinin, V.V.; Sevost'yanov, E.N.; Testov, I.O.; Testov, O.A. Frequency dependence of an electromagnetic absorption coefficient in magnetic fluid. *Tech. Phys.* **2019**, *64*, 893–896. [[CrossRef](#)]
17. Kharitonskii, P.V.; Gareev, K.G.; Ionin, S.A.; Ryzhov, V.A.; Bogachev, Y.V.; Klimenkov, B.D.; Kononova, I.E.; Moshnikov, V.A. Microstructure and magnetic state of Fe<sub>3</sub>O<sub>4</sub>-SiO<sub>2</sub> colloidal particles. *J. Magn.* **2015**, *20*, 221–228. [[CrossRef](#)]
18. Kononova, I.E.; Gareev, K.G.; Moshnikov, V.A.; Al'myashev, V.I.; Kucherova, O.V. Self-assembly of fractal magnetite-silica aggregates in a static magnetic field. *Inorg. Mater.* **2014**, *50*, 68–74. [[CrossRef](#)]
19. Gareev, K.G.; Kononova, I.E.; Levitskii, V.S.; Moshnikov, V.A.; Nalimova, S.S. Influence of constant magnetic field on aggregation processes in magnetite colloids. *J. Phys. Conf. Ser.* **2014**, *572*, 012027. [[CrossRef](#)]
20. Vezo, O.S.; Gareev, K.G.; Korolev, D.V.; Kuryshev, I.A.; Lebedev, S.V.; Moshnikov, V.A.; Sergienko, E.S.; Kharitonskii, P.V. Aggregate stability and magnetic characteristics of colloidal Fe<sub>m</sub>O<sub>n</sub>-SiO<sub>2</sub> particles obtained by Sol-Gel method. *Phys. Solid State* **2017**, *59*, 1008–1013. [[CrossRef](#)]
21. Kharitonskii, P.V.; Gareev, K.G.; Frolov, A.M.; Lebedev, S.V.; Velikorussov, P.V. The investigation of superparamagnetic colloidal particles Fe<sub>m</sub>O<sub>n</sub>-SiO<sub>2</sub>. *Solid State Phenom.* **2016**, *249*, 138–141. [[CrossRef](#)]
22. Gareev, K.G.; Ionin, S.A.; Korolev, D.V.; Luchinin, V.V.; Moshnikov, V.A.; Panov, M.F.; Permyakov, N.V. Study of colloidal particles Fe<sub>m</sub>O<sub>n</sub>-SiO<sub>2</sub> synthesized by two different techniques. *J. Phys. Conf. Ser.* **2015**, *643*, 012088. [[CrossRef](#)]
23. Kharitonskii, P.; Kamzin, A.; Gareev, K.; Valiullin, A.; Vezo, O.; Sergienko, E.; Korolev, D.; Kosterov, A.; Lebedev, S.; Gurylev, A.; et al. Magnetic granulometry and Mössbauer spectroscopy of Fe<sub>m</sub>O<sub>n</sub>-SiO<sub>2</sub> colloidal nanoparticles. *J. Magn. Magn. Mater.* **2018**, *461*, 30–36. [[CrossRef](#)]
24. Kharitonskii, P.; Gareev, K.; Korolev, D.; Sergienko, E. Magnetic properties of Fe<sub>m</sub>O<sub>n</sub>-SiO<sub>2</sub> colloidal nanoparticles: Theoretical and experimental aspects. *AIP Conf. Proc.* **2016**, *1748*, 050009. [[CrossRef](#)]
25. Kharitonskii, P.; Frolov, A.; Gareev, K.; Korolev, D.; Sergienko, E.; Ivanova, E.; Vlasenko, S. The anhysteretic remanent magnetization of magnetite-silica composite nanoparticles. *AIP Conf. Proc.* **2017**, *1874*, 040010. [[CrossRef](#)]
26. Smerdov, R.S.; Bocharova, T.V.; Gareev, K.G. Spectroscopic properties of superparamagnetic Fe<sub>m</sub>O<sub>n</sub>-SiO<sub>2</sub> nanoparticle colloidal solutions. *J. Phys. Conf. Ser.* **2016**, *769*, 012037. [[CrossRef](#)]
27. Gracheva, I.E.; Olchowik, G.; Gareev, K.G.; Moshnikov, V.A.; Kuznetsov, V.V.; Olchowik, J.M. Investigations of nanocomposite magnetic materials based on the oxides of iron, nickel, cobalt and silicon dioxide. *J. Phys. Chem. Sol.* **2013**, *74*, 656–663. [[CrossRef](#)]
28. Gareev, K.G.; Gracheva, I.E.; Moshnikov, V.A. The Sol-Gel method and study of Fe<sub>2</sub>O<sub>3</sub>-NiO-Co<sub>3</sub>O<sub>4</sub>-SiO<sub>2</sub> magnetic nanocomposites. *Glass Phys. Chem.* **2013**, *39*, 548–554. [[CrossRef](#)]
29. Tarasov, S.A.; Gracheva, I.E.; Gareev, K.G.; Gordyushenkov, O.E.; Lamkin, I.A.; Men'kovich, E.A.; Moshnikov, V.A.; Presnyakova, A.V. Atomic force microscopy and photoluminescence analysis of porous metal-oxide materials. *Semiconductors* **2012**, *46*, 1584–1588. [[CrossRef](#)]
30. Afonin, V.; Balbekin, N.S.; Gareev, G.Z.; Gareev, K.G.; Gorshkov, A.N.; Korolev, D.V.; Luchinin, V.V.; Smolyanskaya, O.A. Features of the terahertz spectra of iron oxide nanoparticles in a silicon dioxide shell and of iron oxide and hydroxide nanoparticles. *J. Opt. Technol.* **2017**, *84*, 515–520. [[CrossRef](#)]
31. Smerdov, R.S.; Bocharova, T.V.; Levitskii, V.S.; Gareev, K.G.; Moshnikov, V.A.; Terukov, E.I. Spectroscopic properties of  $\gamma$ -Irradiated Fe<sub>m</sub>O<sub>n</sub>-SiO<sub>2</sub> composite nanoparticles. *Phys. Solid State* **2016**, *58*, 919–923. [[CrossRef](#)]
32. Al'myashev, V.I.; Gareev, K.G.; Ionin, S.A.; Levitskii, V.S.; Moshnikov, V.A.; Terukov, E.I. Investigation of the structure, elemental and phase compositions of Fe<sub>3</sub>O<sub>4</sub>-SiO<sub>2</sub> composite layers by scanning electron microscopy, X-ray spectroscopy, and thermal nitrogen desorption methods. *Phys. Solid State* **2014**, *56*, 2155–2159. [[CrossRef](#)]
33. Gareev, K.G.; Nepomnyashchaya, E.K. Obtaining and characterizing a water-based magnetic fluid. *Bull. Russ. Acad. Sci. Phys.* **2019**, *83*, 904–905. [[CrossRef](#)]

